Open Access, Peer Reviewed, Research Journal

Print & Online available on https://jesbulletin.in
Research Article

Structural Analysis of $Y_3Fe_5O_{12}$ garnet nanoparticles (YIGNPs) Synthesized using Solgel method

*Shaikh Taufiq Khalil Ahmed *[a], Atul D. Saraf[a], Rahul Pandit[a], V.D. Murumkar[c]*

[a]*Department of Physics, Deogiri College, Chhatrapti Sambhajinagar 431001 INDIA*
[b]*Department of Physics, MGM University, Chhatrapti Sambhajinagar 431001 INDIA*
[c]*Department of Physics, Vivekanand Arts, Sardar DalipSingh Commerce and Science College, Chhatrapti Sambhajinagar 431001 INDIA*

Corresponding author: taught9745@gmail.com

ARTICLE INFO

Received: 10/02/2024
Revised: 15/03/2024
Accepted: 01/04/2024

KEYWORDS

Solgel; YIG; Yttrium Iron Garnet; Nanoparticle

ABSTRACT

This study investigates the synthesis and characterization of Yttrium Iron Garnet Nanoparticles (YIGNPs), a subclass of garnet ferrites known for their unique magnetic, optical, and electrical properties. YIGNPs were synthesized using the sol-gel method, which provides precise control over the composition, size, and morphology of the nanoparticles. The X-ray diffraction (XRD) analysis confirmed the formation of a highly crystalline cubic garnet structure, with sharp and well-defined peaks corresponding to the YIG phase. The lattice parameter remained consistent around 12.37 Å, indicating a stable crystal structure, while slight variations were observed in some reflections, suggesting minimal structural changes. The YIGNPs exhibited excellent crystallinity and phase purity, essential for their superior magnetic properties, including low magnetic losses at microwave frequencies. These properties make YIGNPs promising candidates for applications in high-frequency signal processing, quantum computing, and telecommunications. The study demonstrates the potential of garnet ferrites, particularly YIG, as advanced materials for next-generation technologies, offering a platform for further exploration and optimization in various industrial applications

1 Introduction

Garnet ferrites, a subclass of magnetic ceramics, are characterized by their distinct cubic crystal structure and complex composition, which significantly influence their magnetic and optical properties. The general formula for garnet ferrites is $M_3Fe_5O_{12}$, where M typically represents rare-earth elements such as yttrium (Y), gadolinium (Gd), or terbium (Tb). This structure is derived from the natural mineral garnet, specifically the silicate mineral $Mn_3Al_2Si_3O_{12}$, where silicon and manganese are substituted by aluminum and rare-earth ions to form compounds like $Y_3Al_5O_{12}$ [1]. Yttrium iron garnet ($Y_3Fe_5O_{12}$; YIG) is a well-known material with remarkable magnetic, optical, and electrical properties [2]. The unique arrangement of ions within garnet ferrites includes tetrahedral, octahedral, and dodecahedral sites, which contribute to their ferrimagnetic behavior a phenomenon where opposing magnetic moments result in a net magnetization that is weaker than that of ferromagnetic materials [3, 4]. YIG is known for its superior magnetic and magneto-optic behaviors, attributed to the incorporation of yttrium ions that improve structural stability and refine the magnetic properties of the material. YIG's low magnetic losses at microwave frequencies make it especially useful for high-frequency signal processing, where stable and precise magnetic properties are critical. YIG is also being investigated for potential roles in quantum computing, where its low-damping magnetic properties could enhance qubit performance, and in telecommunications, where its ability to control light waves with magnetic fields provides key benefits. Garnet ferrites have a more complex cubic crystal structure than spinel ferrites and incorporate rare-earth elements (e.g., yttrium, gadolinium, terbium), making them highly specialized materials. They are represented by the formula ($M_3Fe_5O_{12}$), where M is a rare-earth ion (M= Y, La, Gd, etc). The cubic unit cell contains 8 formula units or 160 atoms, which can be described as a spatial arrangement of 96 O^{2-} with interstitial cations. The general chemical formula for garnet can also be written more informatively as [5];

$$(R_3)^{c}(Fe_2)^{a}(Fe_3)^{d}O_3 \qquad (1)$$

Here, R = Y, La, Ho, Dy, Gd, Yb, Nd, Sm, Er, Eu, Sc, Ce, Tb, Tm, Pr, Lu. In the above equation, the superscripts c, a, d, refer to the lattice sites such as dodecahedral or {c} - sites, octahedral or [a]-

sites, and tetrahedral or (d)-sites as shown in **Figure 1**. Usually, in the garnets the metallic ions are trivalent. The analogous mineral garnets are silicates of the form $Ca_3{}^{c}\,Fe_2{}^{a}\,Si_3{}^{d}\,O_{12}$. The prototype ferrimagnetic iron garnet is yttrium iron garnet:

$$\{Y_3\}[Fe_2](Fe_3)O_{12} \quad (2)$$

or,

$$Y_3Fe_5O_{12} \quad (3)$$

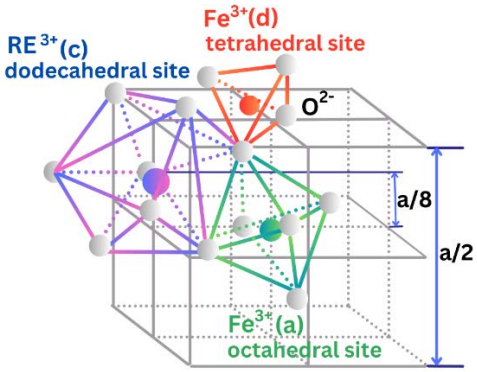

Figure 1 *Crystal structure of garnet ferrite*

Rare earth elements (REEs) have high specificity and value across a range of applications. For instance, europium, indispensable as a red phosphor in color cathode-ray tubes and liquid crystal displays used in computer monitors and televisions, has no known substitutes due to its unique properties and relatively low abundance. In fiber-optic telecommunications, erbium is critical, enabling signal transmission over long distances through erbium-doped fiber sections that act as laser amplifiers, providing greater bandwidth than the copper cables they have largely replaced. The sol-gel method is an attractive synthesis route for producing yttrium garnet [6]. This technique is renowned for its simplicity, cost-effectiveness, and ability to produce homogeneous, fine powders with excellent compositional control [7-9]. By utilizing the sol-gel method, it is possible to achieve uniform and fine particle sizes, which are critical for enhancing the material's properties and ensuring high performance in practical applications. YIGNPs have unique electrical and magnetic properties best suited for high-frequency applications [10]. They are used in magnetic ink [11] and magnetic fluids [12] and for the fabrication of magnetic core of reading and write heads of high-speed digital tapes [13]. These properties make them suitable for various applications like Electro-Magnetic Interference (EMI) suppression [14], canting of the spins [15], superparamagnetic gesture [16], tissue imaging [17], and multimodal diversity [18] biotechnology [19], telecommunication [20] electrical switching applications [21], magnetic recording heads [22], antenna rods [23], microwave devices [24], MLCI [25], power switches, resonators, computer devices [26], TV sets etc. [27]. Some of the important applications include medical diagnosis tools [28], memory chips [29], targeted drug delivery [24], Ni-based batteries [30], MRI [31], sensor [32], spintronics [33, 34], etc. The remarkable properties such as high saturation magnetization, high coercivity, strong anisotropy along with good mechanical hardness, and chemical stability are not observed in the bulk sample [35, 36]. This research aims to investigate the sol-gel synthesis of YIGNPs and to systematically study on the structural, magnetic, and optical properties of the material. By exploring the effects of, this research aims to provide valuable insights into the tunability of yttrium garnet's properties, paving the way for the development of advanced materials with enhanced performance for a wide range of technological applications as shown in **Figure 2**.

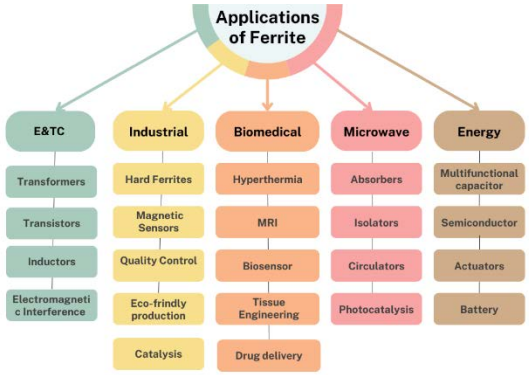

2.1 Materials

YIGNPs were synthesized using the sol-gel method. Stoichiometric amounts of Yttrium nitrate hexahydrate ($Y(NO_3)_3{\cdot}6H_2O$) 383.01 g/mol, Iron (III) nitrate nonahydrate ($Fe(NO_3)_3{\cdot}9H_2O$) 404.00 g/mol were dissolved in distilled water to obtain the desired compositions with . The citric acid ($C_6H_8O_7$) 210.14 g/mol with the nitrate to acid ratio 1:3; acts as a complexing agent, forming metal-citrate complexes that help with homogeneous mixing at the molecular level. NH_3 was used to maintain the Ph at 7.

3 Synthesis

3.1 Solgel synthesis of YIGNPs

In the YIG garnet structure, yttrium acts as the base cation and can be partially substituted with other elements, such as Fe, to tailor the material's properties. Elements from the lanthanide series are often used as substitutes for yttrium to fine-tune the magnetic and optical characteristics of the nanoparticles. Iron, from Group 8 of the periodic table, contributes magnetic properties through its unpaired

d-electrons, while oxygen forms the anionic framework, coordinating with metal cations to ensure structural stability. The sol-gel synthesis process, illustrated in the accompanying flowchart, is a well-established technique for producing $Y_3Fe_5O_{12}$ garnet nanoparticles (YIGNPs) at the nanoscale. This method provides precise control over the composition, size, and morphology of nanoparticles, making them ideal for diverse technological applications. The synthesis begins with the selection of key precursors: yttrium nitrate hexahydrate ($Y(NO_3)_3 \cdot 6H_2O$) supplies yttrium ions essential to the garnet structure, while iron (III) nitrate nonahydrate ($Fe(NO_3)_3 \cdot 9H_2O$) provides the necessary iron ions. Citric acid ($C_6H_8O_7$) serves as a complexing agent, preventing premature aggregation and ensuring a homogeneous mixture. The choice of solvent, such as ethanol or methanol, is also critical, as it must be miscible with the precursors and possess appropriate volatility for efficient drying. During the mixing stage, the precursors are combined into a uniform solution, which is then subjected to aging at approximately 80°C. During this stage, hydrolysis and condensation reactions occur, forming metal hydroxides that link into a three-dimensional network, ultimately leading to gelation and the formation of a wet gel a porous metal oxide structure containing trapped solvent. The wet gel is subsequently dried to form a xerogel, with careful control of the drying process to minimize cracking or shrinkage. Finally, the xerogel undergoes calcination at high temperatures (typically above 500°C), which removes residual organics and facilitates the crystallization of the amorphous phase into the crystalline $Y_3Fe_5O_{12}$ garnet. The calcination temperature and duration are critical factors that influence the final crystallinity, phase purity, and magnetic properties of the nanoparticles. By optimizing each step, researchers can fine-tune the size, morphology, and performance of YIGNPs for applications such as magnetic recording media. The flowchart in Figure 3 depicts the subsequent stages involved in the sol-gel synthesis

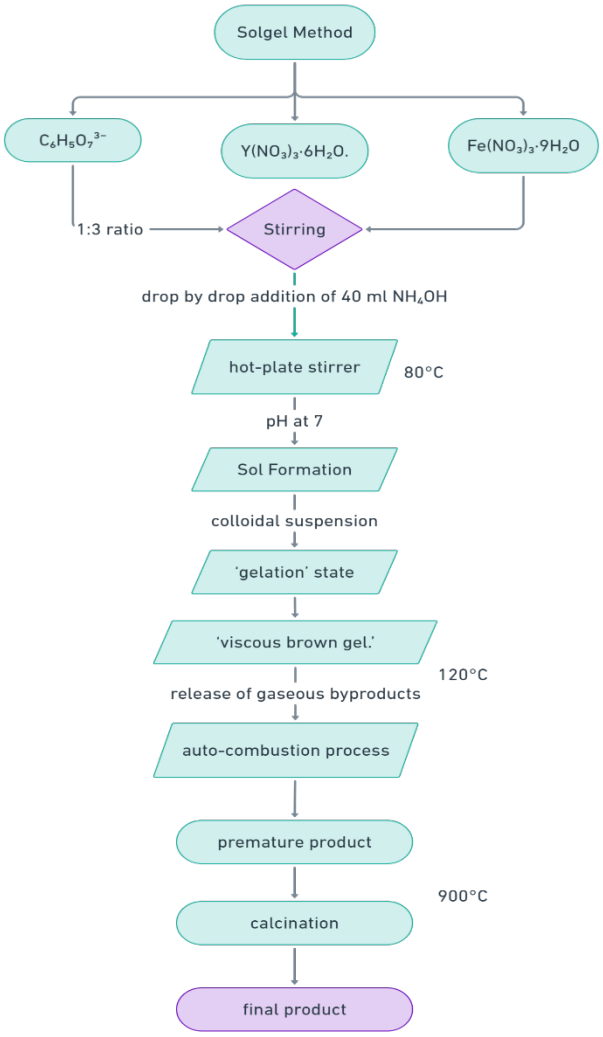

Figure 3 *The subsequent stages involved in the sol-gel synthesis of YIGNPs*

3.2 Chemical reactions during YIGNPs formation

Dissolution and Complexation

Yttrium Nitrate Hexahydrate

$$Y(NO_3)_3 \cdot 6H_2O \rightarrow Y^{3+} + 3NO_3^- + 6H_2O \quad (4)$$

Iron (III) Nitrate Nonahydrate

$$Fe(NO_3)_3 \cdot 6H_2O \rightarrow Fe^{3+} + 3NO_3^- + 9H_2O \quad (5)$$

$$3Y(NO_3)_3 + 5Fe(NO_3)_3 \rightarrow Y_3Fe(NO_3)_{12}\ (in\ solution) \quad (6)$$

Citric acid ($C_6H_8O_7$) chelates the metal ions, forming Metal-Citric Acid Complexes

$$Y^{3+} + Fe^{3+} + C_6H_8O_7 \rightarrow [Y - Citric\ acid] + [Fe - Citric\ acid] \quad (7)$$

Gel formation involves the formation of a metal-organic network, which includes

$$[Y - Citric\ acid] + [Fe - Citric\ acid] + Ammonia\ (NH_3) \rightarrow Gel\ Network\ (Y_3Fe_5(OH)_{12}) \quad (8)$$

Obtain Xerogel

$$Gel\ Network\ (Y_3Fe_5(OH)_{12}) \rightarrow Xerogel\ (Y_3Fe_5(OH)_{12})\ dry \quad (9)$$

Calcination to Form Garnet

$$Xerogel\ (Y_3Fe_5(OH)_{12}) \rightarrow (Y_3Fe_5(OH)_{12}) + H_2O \quad (10)$$

4 Structural property of YIGNPs

YIGNPs, with the chemical symbol $Y_3Fe_5O_{12}$ and CAS number 12063-56-8, comprise elements from specific groups in the periodic table: yttrium from Group 3, iron from Group 8, and oxygen from Group 16. The electronic configurations of these elements are as follows: yttrium (Y) is [Kr] $4d^1\ 5s^2$, iron (Fe) is [Ar] $3d^6\ 4s^2$, and oxygen (O) is $1s^2\ 2s^2\ 2p^4$ [37-39]. The garnet structure is a type of cubic crystal system known for its general formula $AB_3C_2O_{12}$, where the cations occupy specific sites within the crystal lattice. yttrium garnet ($Y_3Fe_5O_{12}$) features a cubic crystal structure typical of Space Group: I4-3d for the garnet structure, characterized by its specific arrangement of metal and oxygen ions. In this structure, yttrium (Y^{3+}) and ions occupy the 8-coordinate dodecahedral (A) sites, while iron (Fe^{3+}) ions are located in the 6-coordinate octahedral (B) sites. The oxygen ions form a three-dimensional framework around these metal ions, contributing to the stability and functionality of the material. The overall crystal lattice of YIGNPs is highly ordered, with the oxygen ions creating a tetrahedral network that interlinks the metal ions. This arrangement results in a stable and robust structure, which is crucial for the material's enhanced magnetic and optical properties. The presence of Y ions introduces additional magnetic anisotropy and shifts in the Curie temperature, while also contributing to distinct optical absorption and emission characteristics due to their 4f-4f electronic transitions. This well-defined structure underpins the material's effectiveness in advanced applications such as optical isolators, microwave devices, and magnetic sensors [40-43].

4.1 X-ray diffraction pattern of YIGNPs

The X-ray diffraction (XRD) pattern of (YIGNPs) in Figure 4 exhibits sharp and well-defined peaks, indicating the formation of a highly crystalline phase. The prominent peaks are indexed to specific crystal planes such as (211), (400), (420), (422), (521), (532), (444), (640), (642), (800), (840), (842), (664), and (868), confirming the cubic garnet structure of YIG [44]. The absence of additional peaks suggests high phase purity, with no detectable impurities or secondary phases like $YFeO_3$ or α-Fe_2O_3. The sharpness and intensity of the peaks further highlight the excellent crystallinity of the nanoparticles, which is crucial for their magnetic and optical properties. The highest intensity peak at the (420) plane suggests a preferred crystallographic orientation along this direction, potentially influencing the anisotropic behavior of the material. The diffraction pattern aligns with standard JCPDS data (e.g., PDF card 43-0507) [45], validating the successful synthesis of the YIG phase. Additionally, the crystallite size can be estimated using the Scherrer equation for more detailed structural analysis.

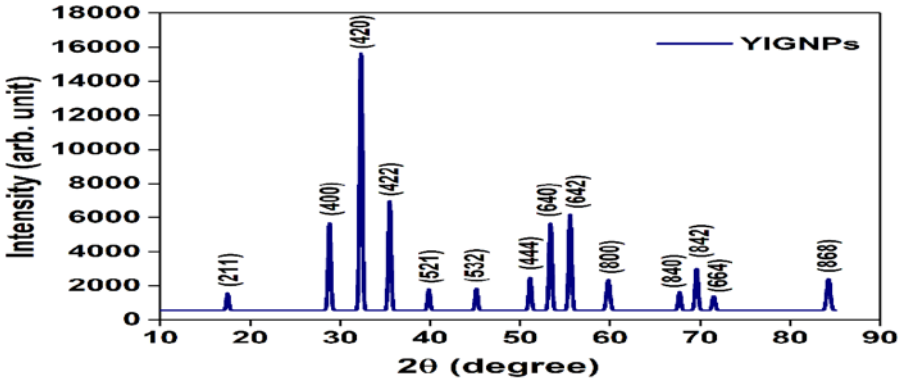

Figure 4 *X-ray diffraction pattern of YIGNPs*

Table 1 Miller indices (hkl), diffraction angle 2θ, interplanner spacing (d), and lattice constant (a) of the YIGNPs

x = 0.0									
h	k	l	2θ	θ	Sinθ	2Sinθ	d	(a/d)^2	a
2	1	1	17.670	8.835	0.154	0.307	5.014	2.793	12.282
4	0	0	28.821	14.410	0.249	0.498	3.094	7.334	12.378
4	2	0	32.317	16.159	0.278	0.557	2.767	9.171	12.375
4	2	2	35.510	17.755	0.305	0.610	2.525	11.011	12.372
5	2	1	39.860	19.930	0.341	0.682	2.259	13.758	12.374
5	3	2	45.150	22.575	0.384	0.768	2.006	17.450	12.366
4	4	4	51.109	25.555	0.431	0.863	1.785	22.034	12.369
6	4	0	53.372	26.686	0.449	0.898	1.715	23.882	12.365
6	4	2	55.553	27.777	0.466	0.932	1.652	25.716	12.366
8	0	0	59.792	29.896	0.498	0.997	1.545	29.417	12.361
8	4	0	67.710	33.855	0.557	1.114	1.382	36.749	12.364
8	4	2	69.609	34.805	0.571	1.142	1.349	38.576	12.366
6	6	4	71.507	35.754	0.584	1.169	1.318	40.425	12.364
8	6	8	84.199	42.100	0.670	1.341	1.149	53.219	14.711
									12.529

The **Table 1** provided table contains the Miller indices (h k l) for various reflections in a material, along with corresponding values for 2θ (the diffraction angle), θ (half the diffraction angle), sinθ, 2sinθ, interplanar distance d, (a/d)2, and the lattice parameter a. The data shows that as the diffraction angle 2θ increases, the interplanar distance d decreases, which is typical in X-ray diffraction. The lattice parameter a remains relatively constant around 12.37 Å across most of the reflections, indicating a stable crystal structure, although there is a slight increase in the last entry (14.711 Å). The values of (a/d)2 generally increase with higher diffraction angles, suggesting a potential relationship between the material's crystalline properties and the diffraction pattern. The consistent lattice parameter suggests that the crystal structure is likely cubic or exhibits minimal variations in lattice spacing. However, the small changes in a could reflect minor structural evolutions, such as thermal expansion. Overall, the data provides a clear picture of the material's crystal structure, with predictable diffraction behavior and a consistent lattice parameter, which can be further analyzed for a more detailed understanding of the crystal's properties.

5 Conclusion

In conclusion, the synthesis and characterization of Yttrium Iron Garnet Nanoparticles (YIGNPs) using the sol-gel method has provided valuable insights into the material's structural, magnetic, and optical properties. The successful formation of the cubic garnet structure, as confirmed by X-ray diffraction (XRD) analysis, indicates high phase purity and excellent crystallinity, essential for the material's superior magnetic performance. The consistent lattice parameter observed in the diffraction data suggests a stable crystal structure, while minor variations may reflect subtle structural changes. These YIGNPs, with their remarkable magnetic properties, such as low magnetic losses at microwave frequencies, hold great potential for high-frequency signal processing, quantum computing, and telecommunications. The ability to fine-tune their properties through controlled synthesis and elemental substitution makes them highly versatile for a wide range of technological applications. Overall, the research highlights the promise of garnet ferrites, particularly YIG, as advanced materials for cutting-edge applications in electronics and quantum technologies.

Reference

[1] M.N. Akhtar, M.A. Khan, M. Ahmad, G. Murtaza, R. Raza, S. Shaukat, M. Asif, N. Nasir, G. Abbas, M. Nazir, Y3Fe5O12 nanoparticulate garnet ferrites: comprehensive study on the synthesis and characterization fabricated by various routes, Journal of magnetism and magnetic materials, 368 (2014) 393-400.

[2] S. Nimbore, D. Shengule, S. Shukla, G. Bichile, K. Jadhav, Magnetic and electrical properties of lanthanum substituted yttrium iron garnets, Journal of materials science, 41 (2006) 6460-6464.

[3] T. Aichele, A. Lorenz, R. Hergt, P. Görnert, Garnet layers prepared by liquid phase epitaxy for microwave and magneto-optical applications–a review, Crystal Research and Technology: Journal of Experimental and Industrial Crystallography, 38 (2003) 575-587.

[4] Y. Yang, T. Liu, L. Bi, L. Deng, Recent advances in development of magnetic garnet thin films for applications in spintronics and photonics, Journal of Alloys and Compounds, 860 (2021) 158235.

[5] R.J. Angel, M. Gilio, M. Mazzucchelli, M. Alvaro, Garnet EoS: a critical review and synthesis, Contributions to Mineralogy and Petrology, 177 (2022) 54.

[6] A. Leleckaite, A. Kareiva, Synthesis of garnet structure compounds using aqueous sol–gel processing, Optical Materials, 26 (2004) 123-128.

[7] S. Bashir, J. Liu, Overviews of synthesis of nanomaterials, Advanced nanomaterials and their applications in renewable energy: Elsevier Science, DOI (2015) 51-115.

[8] A.V. Raut, P.P. Khirade, D. Shengule, K. Jadhav, 50 kGy–100 kGy 60 Co γ-irradiation effects on structural and DC-electrical properties of sol–gel synthesized ZnF NPs, Journal of Materials Science: Materials in Electronics, 32 (2021) 11017-11027.

[9] W.A. Alwesabi, P.D. Dange, A.V. Raut, G.M. Puri, R.M. Khobragade, P.P. Pawar, S. Pammi, C.K. Kumar, P. Kollu, Microstructural, Optical, and Antimicrobial Activity of ZnO-CuO NCP Prepared Using Co-precipitation Technique, Journal of Superconductivity and Novel Magnetism, DOI (2024) 1-15.

[10] W. Li, W. Wang, J. Lv, Y. Ying, J. Yu, J. Zheng, L. Qiao, S. Che, Structure and magnetic properties of iron-based soft magnetic composite with Ni-Cu-Zn ferrite–silicone insulation coating, Journal of Magnetism and Magnetic Materials, 456 (2018) 333-340.

[11] M. Vaseem, F.A. Ghaffar, M.F. Farooqui, A. Shamim, Iron Oxide Nanoparticle-Based Magnetic Ink Development for Fully Printed Tunable Radio-Frequency Devices, Advanced Materials Technologies, 3 (2018) 1700242.

[12] P. Pradhan, J. Giri, G. Samanta, H.D. Sarma, K.P. Mishra, J. Bellare, R. Banerjee, D. Bahadur, Comparative evaluation of heating ability and biocompatibility of different ferrite-based magnetic fluids for hyperthermia application, Journal of Biomedical Materials Research Part B: Applied Biomaterials: An Official Journal of The Society for Biomaterials, The Japanese Society for Biomaterials, and The Australian Society for Biomaterials and the Korean Society for Biomaterials, 81 (2007) 12-22.

[13] G.R. Skutt, F.C. Lee, Characterization of dimensional effects in ferrite-core magnetic devices, PESC Record. 27th Annual IEEE Power Electronics Specialists Conference, IEEE, 1996, pp. 1435-1440.

[14] D. Shin, S. Jeong, J. Kim, Quantified design guidelines of a compact transformerless active EMI filter for performance, stability, and high voltage immunity, IEEE Transactions on Power Electronics, 33 (2017) 6723-6737.

[15] M.P. Ghosh, S. Mukherjee, Canted surface spins driven exchange anisotropy in erbium substituted nickel ferrite nanoparticles, Materials Characterization, 162 (2020) 110203.

[16] S.B. Somvanshi, S.A. Jadhav, M.V. Khedkar, P.B. Kharat, S. More, K. Jadhav, Structural, thermal, spectral, optical and surface analysis of rare earth metal ion (Gd3+) doped mixed Zn–Mg nano-spinel ferrites, Ceramics International, DOI (2020).

[17] S.O. Aisida, I. Ahmad, T.-k. Zhao, M. Maaza, F.I. Ezema, Calcination Effect on the Photoluminescence, Optical, Structural, and Magnetic Properties of Polyvinyl Alcohol Doped ZnFe2O4 Nanoparticles, Journal of Macromolecular Science, Part B, 59 (2020) 295-308.

[18] D. Rawat, P. Barman, R.R. Singh, Multifunctional magneto-fluorescent NiZnFe@ CdS core-shell nanostructures for multimodal applications, Materials Chemistry and Physics, 231 (2019) 388-396.

[19] R. Haghniaz, A. Rabbani, F. Vajhadin, T. Khan, R. Kousar, A.R. Khan, H. Montazerian, J. Iqbal, A. Libanori, H.-J. Kim, Anti-bacterial and wound healing-promoting effects of zinc ferrite nanoparticles, Journal of Nanobiotechnology, 19 (2021) 1-15.

[20] T. Vigneswari, P. Raji, Structural and magnetic properties of calcium doped nickel ferrite nanoparticles by co-precipitation method, Journal of Molecular Structure, 1127 (2017) 515-521.

[21] A. Hao, D. Jia, M. Ismail, R. Chen, D. Bao, Controlling of resistive switching and magnetism through Cu2+ ions substitution in nickel ferrite based nonvolatile memory, Journal of Alloys and Compounds, 790 (2019) 70-77.

[22] K. Ugendar, G. Markandeyulu, S. Mallesh, Polaron conduction mechanism in Nickel ferrite and its rare-earth derivatives, Physica B: Condensed Matter, DOI (2021) 412819.

[23] V. Singh, A. Rajagopalan, A. Peralta, M.N. Alam, C.A. Frysz, J. Luzinski, G. Riese, J. Babcock, P. Shostak, Multi-mode wireless antenna configurations, Google Patents, 2021.

[24] S. Yattinahalli, S. Kapatkar, N. Ayachit, S. Mathad, Synthesis and structural characterization of nanosized nickel ferrite, International Journal of Self-Propagating High-Temperature Synthesis, 22 (2013) 147-150.

[25] M.P. Reddy, G. Balakrishnaiah, W. Madhuri, M.V. Ramana, N.R. Reddy, K.S. Kumar, V. Murthy, R.R. Reddy, Structural, magnetic and electrical properties of NiCuZn ferrites prepared by microwave sintering method suitable for MLCI applications, Journal of Physics and Chemistry of Solids, 71 (2010) 1373-1380.

[26] A. Ghatage, S. Choudhari, S. Patil, S. Paranjpe, X-ray, infrared and magnetic studies of chromium substituted nickel ferrite, Journal of materials science letters, 15 (1996) 1548-1550.

[27] M. Shakil, U. Inayat, M. Arshad, G. Nabi, N. Khalid, N. Tariq, A. Shah, M. Iqbal, Influence of zinc and cadmium co-doping on optical and magnetic properties of cobalt ferrites, Ceramics International, 46 (2020) 7767-7773.

[28] S. Joshi, V.B. Kamble, M. Kumar, A.M. Umarji, G. Srivastava, Nickel substitution induced effects on gas sensing properties of cobalt ferrite nanoparticles, Journal of Alloys and Compounds, 654 (2016) 460-466.

[29] M. Banerjee, A. Mukherjee, S. Chakrabarty, S. Basu, M. Pal, Bismuth-Doped Nickel Ferrite Nanoparticles for Room Temperature Memory Devices, ACS Applied Nano Materials, 2 (2019) 7795-7802.

[30] H. Zhao, Z. Zheng, K.W. Wong, S. Wang, B. Huang, D. Li, Fabrication and electrochemical performance of nickel ferrite nanoparticles as anode material in lithium ion batteries, Electrochemistry communications, 9 (2007) 2606-2610.

[31] N. Sattarahmady, M. Heidari, T. Zare, M. Lotfi, H. Heli, Zinc–nickel ferrite nanoparticles as a contrast agent in magnetic resonance imaging, Applied Magnetic Resonance, 47 (2016) 925-935.

[32] C.G. Reddy, S. Manorama, V. Rao, Semiconducting gas sensor for chlorine based on inverse spinel nickel ferrite, Sensors and Actuators B: Chemical, 55 (1999) 90-95.

[33] S. Anjum, G.H. Jaffari, A.K. Rumaiz, M.S. Rafique, S.I. Shah, Role of vacancies in transport and magnetic properties of nickel ferrite thin films, Journal of Physics D: Applied Physics, 43 (2010) 265001.

[34] S. Bader, S. Parkin, Spintronics, ARCMP, 1 (2010) 71-88.

[35] Y. Shi, J. Ding, Strong unidirectional anisotropy in mechanically alloyed spinel ferrites, Journal of Applied Physics, 90 (2001) 4078-4084.

[36] L. Kumar, M. Kar, Influence of Al3+ ion concentration on the crystal structure and magnetic anisotropy of nanocrystalline spinel cobalt ferrite, Journal of Magnetism and Magnetic Materials, 323 (2011) 2042-2048.

[37] I.H. Hasan, M.N. Hamidon, A. Ismail, I. Ismail, A.S. Mekki, M.A.M. Kusaimi, S. Azhari, R. Osman, YIG thick film as substrate overlay for bandwidth enhancement of microstrip patch antenna, IEEE Access, 6 (2018) 32601-32611.

[38] S. Geller, M. Gilleo, The crystal structure and ferrimagnetism of yttrium-iron garnet, Y3Fe2 (FeO4) 3, Journal of Physics and Chemistry of solids, 3 (1957) 30-36.

[39] S. NISHIKAWA, Crystal structure of a garnet, Proceedings of the Tokyo Mathematico-Physical Society. 2nd Series, 9 (1917) 194-197.

[40] G.J. Redhammer, G. Tippelt, A. Portenkirchner, D. Rettenwander, Aging Behavior of Al-and Ga-Stabilized Li7La3Zr2O12 Garnet-Type, Solid-State Electrolyte Based on Powder and Single Crystal X-ray Diffraction, Crystals, 11 (2021) 721.

[41] L. Néel, R. Pauthenet, B. Dreyfus, Chapter VII the rare earth garnets, Progress in Low Temperature Physics, Elsevier1964, pp. 344-383.

[42] D. Chen, Y. Yang, C. Chen, Y. Meng, Y. Zhang, C. Zhang, Structure and magnetism of novel high-entropy rare-earth iron garnet ceramics, Ceramics International, 49 (2023) 9862-9867.

[43] L. Duan, D. Yang, Z. Wang, R. Su, C. He, X. Yang, X. Long, Growth and characterization of holmium-doped yttrium iron garnet single crystal, Journal of Alloys and Compounds, 966 (2023) 171527.

[44] G. Magno, V. Yam, B. Dagens, Integration of Plasmonics Structures in Photonics Waveguides: Enabling Novel Electromagnetic Functionalities in Photonic Circuits, DOI (2023).

[45] A. Arsad, N. Ibrahim, Temperature-dependent magnetic properties of YIG thin films with grain size less 12 nm prepared by a sol-gel method, Journal of Magnetism and Magnetic Materials, 462 (2018) 70-77.